Improving CdSeTe Devices With a Back Buffer Layer of Cu_xAlO_y

Manoj K. Jamarkattel, Adam B. Phillips, Kamala Khanal Subedi, Ebin Bastola, Jacob M. Gibbs, Jared D Friedl, Suman Rijal, Dipendra Pokhrel, Rasha A. Awni, Deng-Bing Li, John Farrell, Robert F. Klie, Xavier Mathew, Yanfa Yan, Randy J. Ellingson, and Michael J. Heben

***Abstract*—The open-circuit voltage (V_{oc}) of CdTe-based photovoltaics may be limited by carrier recombination at interfaces (front or back) or in the absorber layer. Reduction in recombination of a given dominant mechanisms can lead to improved device performance if the remaining mechanisms turn ON in a narrow bias range just below the open circuit voltage. In this article, we demonstrate enhanced performance by incorporating solution-processed Cu_xAlO_y to form a back-buffer layer in CdSe/CdTe devices. Outstanding minority carrier lifetimes of 656 and 4.2 ns were measured with glass side and film side illumination for device stacks processed with Cu_xAlO_y. Devices demonstrated efficiencies of up to 17.4% with V_{oc} of 859 mV, FF of 75.6% and J_{sc} of 26.9 mAcm^{-2} while the efficiency of the reference device without the back-buffer layer was 16.5% with V_{oc} of 839 mV, FF of 70.6%, and J_{sc} of 27.9 mAcm^{-2}.**

***Index Terms*—Back-contact, CdSeTe, Cu_xAlO_y, passivation.**

I. Introduction

REPLACING the traditional CdS window layer with CdSe in CdTe based polycrystalline solar cells has resulted in higher current collection and higher minority carrier lifetime [1]–[3], both of which allow for significantly better device performance. While there is the potential for V_{OC} greater than 1 V and efficiency over 25% [4], the record V_{OC} and efficiency are only 887 mV and 22.1% [5], respectively. Modeling shows that bulk carrier lifetime may need to be ∼100 ns or longer to achieve 25% [6]. As the bulk lifetime gets longer, it is likely that the measured carrier lifetime will be affected by recombination at the back interface. In fact, studies of carrier lifetimes can provide information about the interface recombination rates [7]. In general, the interplay between carrier recombination at the front and back interfaces, the bulk of the absorber, or at grain boundaries limit the $V_{OC,}$ and the way in which the various mechanisms turn-ON with bias will limit the FF [8].

Recently, MgZnO was incorporated at the front of MgZnO/CdSeTe/CdTe devices in an effort to reduce recombination at the front [9]. This resulted in a carrier lifetime of 256 ns and device efficiency and V_{oc} of 17%–18% and 843 mV, respectively. These improvements are attributed to the formation of tellurium oxide species at the front interface and larger CdSeTe grains, both of which help reduce front and bulk recombination in the device. Although the long carrier lifetimes are promising, the low V_{oc} suggests recombination losses elsewhere in the device, likely at the back interface.

Efforts to reduce recombination at the back interface are underway. Back buffer layers such as CdZnTe, Te nanowires, ZnTe [10]–[13] and oxides TiO_2, Al_2O_3, SiO_2, and Ta_2O_5 [14]–[19] have been applied to improve the hole transport or minimize the carrier recombination at the back surface. Among them, Al_2O_3 has shown back surface passivation resulting in carrier lifetime of 750 ns when CdSeTe was examined in a double heterostructure [20]. Recently, Cu_xAlO_y has been used as a back-buffer layer in CdS/CdTe devices and showed promising results when illuminated through the back interface [21]. Time resolved photoluminescence (TRPL) measurements showed an increase in carrier lifetime when Cu_xAlO_y was incorporated as a back-buffer layer. However, the best carrier lifetime for those device stacks was only on the order of tens of nanoseconds when illuminated from the glass side, and ∼3.4 ns when measured with back illumination. This is likely due to the use of CdS at the front of the device, which is expected to have poor band alignment with CdTe [22]. Further, the solubility of CdS in CdTe is lower than that of CdSe and hence the achievable defect passivation in the bulk is also lower with CdS [23].

Here, we investigate using the solution processed Cu_xAlO_y to reduce back surface recombination in CdSe/CdTe devices. When this material is incorporated into the back of the device, the

Manuscript received June 15, 2021; revised September 5, 2021; accepted October 12, 2021. Date of publication November 4, 2021; date of current version December 23, 2021. This work was supported in part by the research sponsored by Air Force Research Laboratory under Grant FA9453-18-2-0037 and Grant FA9453-19-C-1002 and in part by the U.S. DOE's Office of Energy Efficiency and Renewable Energy under Solar Energy Technologies Office under Agreement DE-EE0008974. *(Corresponding author: Michael J. Heben.)*

Manoj K. Jamarkattel, Adam B. Phillips, Kamala Khanal Subedi, Ebin Bastola, Jacob M. Gibbs, Jared D Friedl, Suman Rijal, Dipendra Pokhrel, Rasha A. Awni, Deng-Bing Li, Yanfa Yan, Randy J. Ellingson, and Michael J. Heben are with the Wright Center for Photovoltaic Innovation and Commercialization, University of Toledo, Toledo, OH 43606 USA (e-mail: manoj.jamarkattel@rockets.utoledo.edu; Adam.Phillips@utoledo.edu; kamala.khanalSubedi@rockets.utoledo.edu; Ebin.Bastola@rockets.utoledo.edu; jacob.gibbs@rockets.utoledo.edu; Jared.Friedl@rockets.utoledo.edu; suman.rijal@rockets.utoledo.edu; dipendra.pokhrel@utoledo.edu; rasha.awni@utoledo.edu; Dengbing.Li@utoledo.edu; yanfa.yan@utoledo.edu; Randy.Ellingson@utoledo.edu; Michael.Heben@utoledo.edu).

John Farrell and Robert F. Klie are with the Department of Physics, University of Illinois at Chicago, Chicago, IL 60607 USA (e-mail: jjfarre2@uic.edu; rfklie@uic.edu).

Xavier Mathew is with the Wright Center for Photovoltaic Innovation and Commercialization, University of Toledo, Toledo, OH 43606 USA, and also with the Instituto de Energías Renovables, Universidad Nacional Autónoma de México, Morelos 62580, México (e-mail: Xavier.Mathew@utoledo.edu).

Color versions of one or more figures in this article are available at https://doi.org/10.1109/JPHOTOV.2021.3120506.

Digital Object Identifier 10.1109/JPHOTOV.2021.3120506

device efficiency exceeds 17% and an excellent minority carrier lifetime greater than 650 ns was measured through the glass. We discuss how this back buffer affects the photoluminescence (PL) and TRPL responses of the absorber, current density-voltage (*J–V*) characteristics, and external quantum efficiency (EQE).

II. Experimental Details

To fabricate these devices, we deposited a bilayer of CdSe/CdTe onto cleaned F-doped SnO_2/glass (Tec 12D; Pilkington North America). First, 150 nm of CdSe was sputtered onto the substrate at room temperature under 10 mTorr Ar pressure. This was followed by depositing 3.5 μm of CdTe using a high vacuum close-space sublimation (CSS) system in which the source and substrate temperatures were 560 °C and 450 °C, respectively, while the chamber pressure was held at 2×10^{-6} Torr. All the coupons were subjected to our standard activation process, which utilizes 100 μL of saturated $CdCl_2$ solution applied directly onto the as-deposited bilayer film stack. After drying, the coupons were annealed at 400 °C for 30 minutes in dry air followed by repeated rinsing with methanol to remove excess $CdCl_2$.

The reference devices were Cu doped by dipping in 0.1 mmol $CuCl_2$ solution in water for 2 min [24]. Upon removal, the coupon was rinsed with DI water, dried with nitrogen, and annealed in an oven at 200 °C for 20 min in ambient air. Cu_xAlO_y was deposited by applying 50 μl of a precursor solution consisting of a 7:3 ratio of 40 mM concentrated aluminum nitrate nonahydrate and 40 mM concentrated copper nitrate trihydrate, dissolved in two-methoxyethanol to the sample [21]. The sample was then spun at 100 r/min for 10 s followed by 50 s at 3500 r/min. Samples were then heated to 220 °C for 6 min on a hot plate to convert the precursor into Cu_xAlO_y. No additional Cu doping was used in these samples.

To complete the devices for *J–V* measurements, 50 nm of gold was evaporated through a mask with cell area of 0.08 cm^2, and the *J–V* characteristics were measured with a Keithley 2440 source meter and an LED solar simulator (Newport Minisolo model LHS-7320) under AM1.5G spectrum. EQE data was also measured (PV measurements Inc.).

Prior to depositing Au, glass side PL measurements were performed using a continuous wave laser operating at 633 nm with a beam diameter of 180 μm and an incident power density of 55 mW/cm^2. Film side PL measurements were performed using the same laser but with a higher power density of 283.9 mW/cm^2. For TRPL measurements, a 633 nm pulsed laser with a beam diameter of 150 μm was used to excite the carriers. The power and repetition rates were chosen to ensure low injection to avoid any artifacts in the measurement. For glass side illuminated measurements, the laser power was 9.5 μW, the repetition rate was 20 MHz, and the photon fluence was 4.5×10^{10} photons/cm^2. The corresponding parameters for film side measurements were 11.6 μW, 20 MHz and 1.1×10^{10} photons/cm^2, respectively.

III. Results and Discussion

Representative scanning electron microscopy (SEM) images of the surfaces are shown in Fig. 1. As-deposited CdTe grains

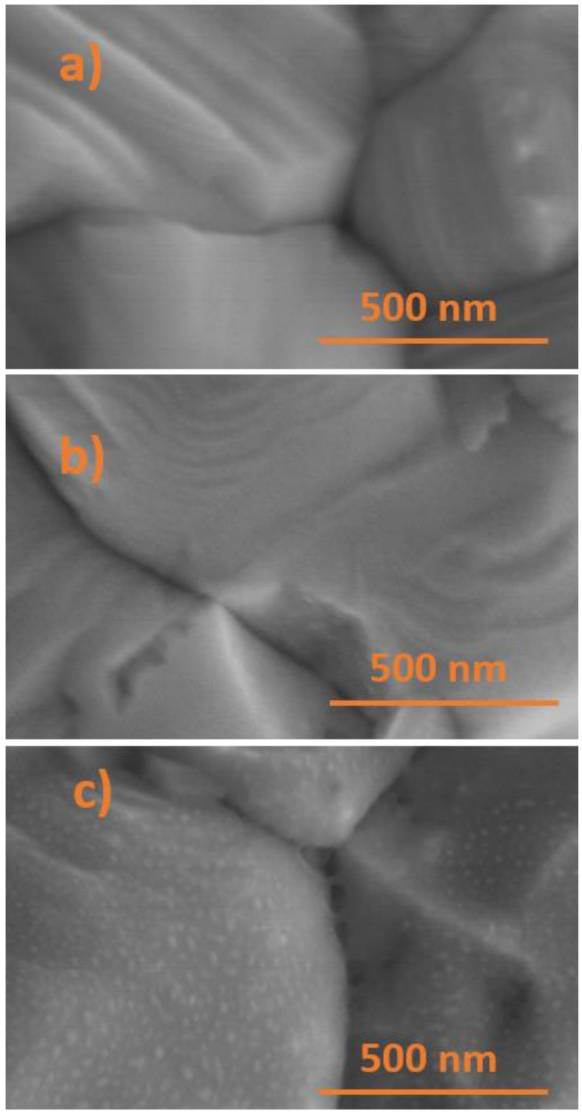

Fig. 1. Surface SEM images of CdTe grains. (a) As deposited CdTe. (b) After $CdCl_2$ and Cu doping. (c) After deposition of Cu_xAlO_y.

are 2–3 μm in size [see Fig. 1(a)] and appear unchanged after $CdCl_2$ processing and Cu doping [see Fig. 1(b)]. However, small features are visible on the CdTe grains [see Fig. 1(c)] after the application of Cu_xAlO_y. The small nodules appear uniform in size and evenly distributed. These structures are similar to those observed in our previous work on Cu_xAlO_y applied to CdS/CdTe devices [21].

However, in this article, we performed TOF-SIMS analysis and high-resolution cross-sectional imaging of the interface to gain a more detailed understanding of the deposited material. Fig. 2 shows a comparison between the surface density of Cu and Al isotopes for a reference sample [see Fig. 2(a) and (b)] and a sample on which Cu_xAlO_y was deposited [see Fig. 2(c) and (d)]. We first note that the surface concentration of Cu was higher by ~3x for the Cu_xAlO_y sample. Also, while the Cu and Al signals are correlated to some degree, the ratio of Cu to Al does not appear to be 1:1, the film is not continuous, and the apparent thickness, where present, is on the order of a

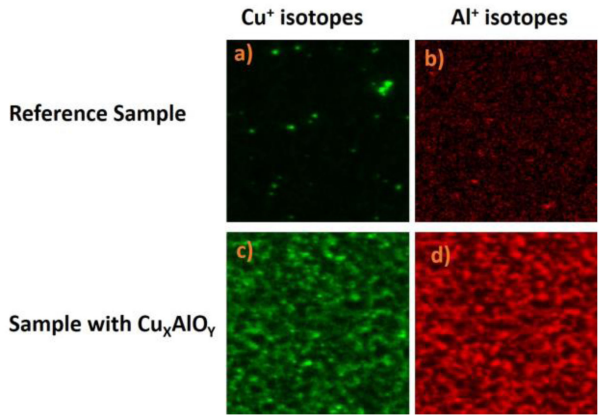

Fig. 2. TOF-SIMS surface images of Cu (a) and (c) and Al isotopes (b) and (d) from a reference sample doped with Cu via $CuCl_2$ (a) and (b) and a sample on which Cu_XAlO_y was deposited (c) and (d).

few nm. Interestingly, the Cu concentration in the depth profiles (not shown) decayed to lower values in the case of Cu_xAlO_y as compared to the $CuCl_2$ dipped sample. This result was confirmed by *C–V* analysis, where the carrier concentrations after $CuCl_2$ doping and Cu_xAlO_y deposition were measured to be 4.5×10^{13} cm^{-3} and 3.0×10^{13} cm^{-3}, respectively. Thus, the degree of doping is marginally higher in the case of $CuCl_2$. The TOF-SIMS data also revealed that the Al depth profile was correlated with the Cu profile in the case of the Cu_xAlO_y sample but, once again, not apparently in a 1:1 fashion. This data needs to be viewed with some caution, however, since the raw ion counts were uncorrected. The Se gradient was found to be similar in both samples.

The back contact interface was also examined by energy-dispersive X-ray spectroscopy using cross-sectional scanning transmission electron microscopy after lifting-out a lamella from a completed device. Interestingly, evidence for the formation of a thin copper-containing AuAl intermetallic layer was observed. Clearly, more studies are required to develop a detailed understanding of the deposited material and the resulting interfaces.

To investigate how the Cu_xAlO_y deposition affected recombination in the device stack, we measured glass side and film side PL and TRPL. Fig. 3 shows the data for device stacks with and without Cu_xAlO_y. For the sample with Cu_xAlO_y, we observed noticeable improvement in the PL intensity with illumination from the glass side [see Fig. 3(a)]. The peak PL intensity of the sample with Cu_xAlO_y was 227% and 48% higher than that of the reference sample before and after $CuCl_2$ doping, respectively [see Fig. 3(a)]. To develop an estimate of the improvement in V_{oc} that should accompany this increase in PL intensity, we consider (1) that holds for low-injection excitation [25], [26]

$$\Delta V_{\mathrm{OC}} = \mathrm{KT}/q * \ln\left(\frac{\mathrm{PLQE}, \mathrm{Cu_xAlO_y}}{\mathrm{PLQE}, \mathrm{Ref}}\right). \quad (1)$$

The ratio of $\mathrm{PLQE_{CuxAlOy}/PLQE_{Ref}} = 1.47$, calculated by taking the area under the corresponding PL bands, yields a value for ΔV_{oc} of $\sim$10 mV improvement, which is consistent with *J–V* findings (*vide infra*).

TABLE I
TRPL DATA OF THE SAMPLES WITH AND WITHOUT BACK BUFFER LAYER

Samples	Glass side Lifetime (ns)	Film side Lifetime (ns)
$CdSe/CdTe/CdCl_2$	293.8	2.2
$CdSe/CdTe/CdCl_2/CuCl_2$	501.4	1.6
$CdSe/CdTe/CdCl_2/Cu_xAlO_y$	656.5	4.2

Turning to the film side PL spectra [see Fig. 3(c)], we note that each sample shows a dominant emission band at 1.38 eV, corresponding to emission from CdSeTe, and a weaker band at 1.49 eV which is attributed to pure CdTe present at the back. After $CdCl_2$ treatment the film side PL is relatively bright, but only $\sim$40% of the intensity as compared to glass side measurement of the same sample. Significant quenching of the PL was observed after $CuCl_2$ treatment, while the sample with Cu_xAlO_y exhibits a PL spectrum which was nearly unchanged relative to the spectrum after $CdCl_2$ treatment. Note that bright and long-live film side PL is an important diagnostic for the development of bifacial devices [17], [19], [28]. The fact that the Cu_xAlO_y deposition yields higher film side PL in comparison to $CuCl_2$ treated samples suggests that the minority carrier recombination rate is lower at the back surface, possibly due to changes in the rear surface band bending. Consistently, the reduced carrier concentration found for the case of Cu_xAlO_y suggests a bigger depletion with at the back of the device. In any case, it seems clear that the electronic processes are different at and near the back interface. Clearly, more work is required to develop a deeper understanding of the related chemistry and physics.

It is also interesting to note the glass side and film side TRPL data [see Fig. 3(b) and (d)]. Biexponential Gaussian fits to the TRPL decay curves were analyzed to obtain carrier lifetimes for the fast decaying component (τ_1) that corresponds to charge redistribution and the slow component (τ_2) which relates to carrier recombination [7]. The data presented in Table I shows that carrier recombination lifetimes (τ_2) measured at the front side of devices without a back buffer is markedly higher than that reported elsewhere [9], [28]. The quality of the material and the degree of passivation at the front interface appears excellent which could be a consequence of the CSS instrument used here, which includes high vacuum pump-out capabilities and a base pressure approaching 1×10^{-8} Torr. The addition of Cu_xAlO_y leads to a significant improvement in the front side lifetime, once again suggesting a reduction in the rear surface recombination rate. Consistently, the τ_2 back side lifetime is also the longest for the Cu_xAlO_y sample.

More quantitative information can be gleaned by assuming that the band-edges are away from the equilibrium condition after the pulsed excitation and that the carriers are redistributed in the space charge region. Under these conditions the recombination rate model suggested by Kuciauskas *et al.* [7] can be written as

$$\frac{1}{\tau 2, \mathrm{TRPL}} = \frac{1}{\tau B} + \frac{1}{\tau \mathrm{front}} + \frac{1}{\tau \mathrm{back}} + \frac{1}{\tau \mathrm{rad}} \quad (2)$$

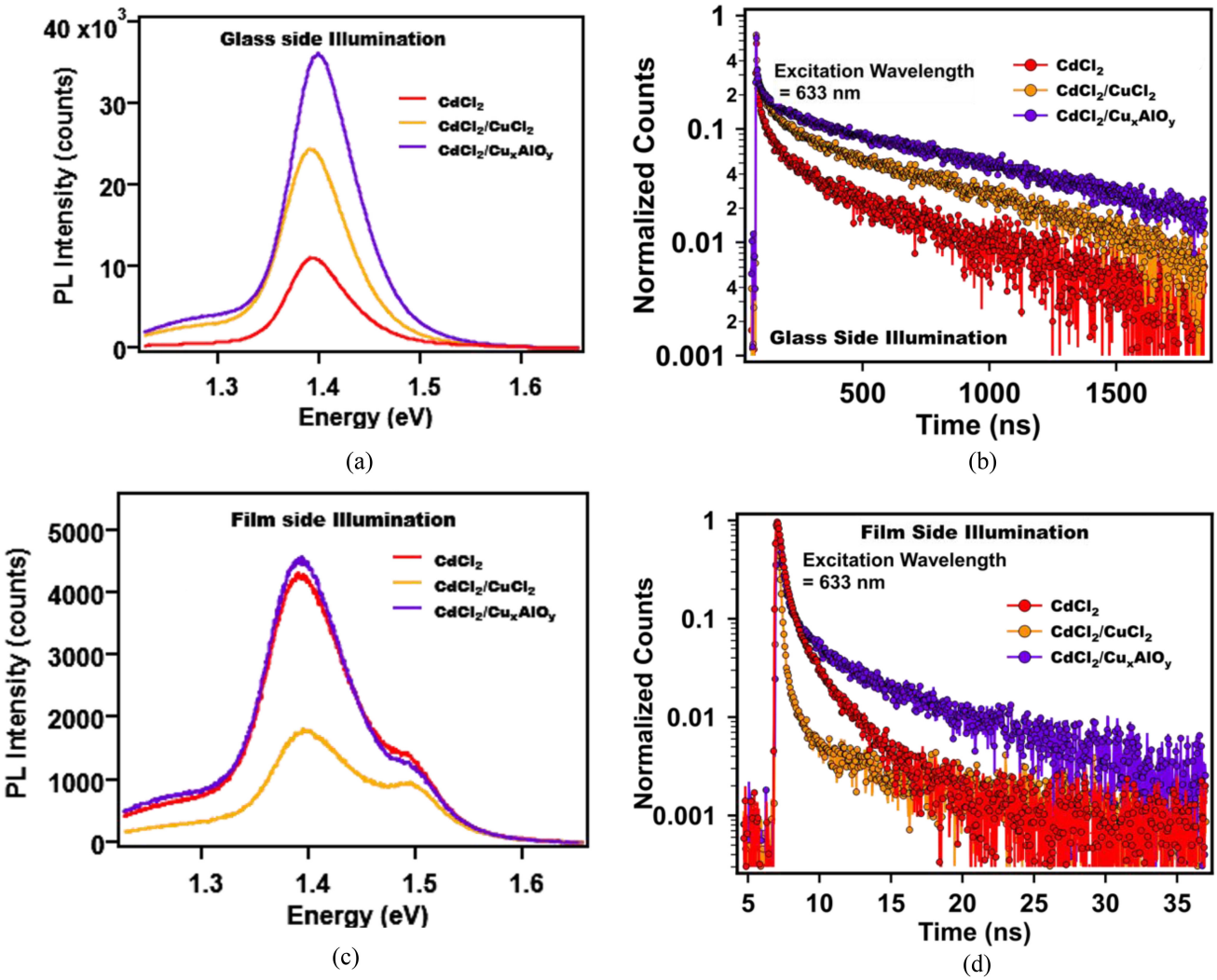

Fig. 3. PL emission spectra and decay curves recorded from PL and TRPL measurements. (a) PL excited through glass side. (b) TRPL excited through glass side. (c) PL excited through film side. (d) TRPL excited through film side.

where τ_B is the bulk Shockley-Reed Hall recombination lifetime, τ_{rad} is the radiative lifetime, and τ_{front} and τ_{back} are the front and back interface recombination lifetimes, respectively. We assume that in both devices the front and bulk properties remain identical while only the back interface is modified with the addition of the buffer layer. Hence, based on this assumption, the difference in effective surface recombination velocity between the reference $CuCl_2$ treated ($S_{\mathrm{back,Ref}}$) device and the samples with Cu_xAlO_y ($S_{\mathrm{back,\ CuxAlOy}}$) can be related to the carrier lifetimes at the different interfaces as shown in

$$(S_{\mathrm{back,Ref}} - S_{\mathrm{back,CuxAlOy}}) = d * \left(\frac{1}{\tau 2, \mathrm{Ref}} - \frac{1}{\tau 2, \mathrm{Cu_xAlO_y}} \right) \quad (3)$$

where d is thickness of CdTe. Using the values of $\tau_{2\ \mathrm{Ref}}$ and $\tau_{2\ \mathrm{CuxAlOy}}$ from Table I the quantity on the righthand side of the equation can be evaluated to be 165 cm/s. Taking the value of $S_{\mathrm{back,Ref}}$ from literature for unpassivated CdTe (1000 cm/s) [7], it follows that the value for $S_{\mathrm{back,\ Cu_xAlO_y}}$ is 835 cm/s. However, it should be mentioned that any possible change in band bending is not taken into account in this discussion [21]. Further, the carrier lifetime value used for the reference device in our analysis is 501.4 ns, while the value used in [7] was 181 ns [7].

To further investigate how the back-buffer layer affects the device performance, *J–V* and EQE measurements were conducted. Fig. 4 shows the *J–V* graphs and the EQE measured at short circuit for each of the champion cells. Fig. 5 shows the box plots of PV parameters averaged for the ten best performing devices. PV parameters of the champion cell with Cu_xAlO_y are V_{oc} of 859 mV, J_{sc} 26.7 $\mathrm{mAcm^{-2}}$, FF 75.6% and efficiency 17.4%. For the best reference device with Cu doping the PV parameters are V_{oc} 839 mV, J_{sc} 27.9 $\mathrm{mAcm^{-2}}$, FF 70.6% and efficiency 16.5%.

In terms of average performance, there is a gain of 12 mV in V_{oc}, which is consistent with the 10 mV value estimated from analysis of the increase in the PL emission band intensity. Additionally, the average FF improved by 3% points, and the overall efficiency improved by an absolute amount of 0.7%.

The EQE shows a relatively flat response across the entire wavelength range. The short wavelength response of the device

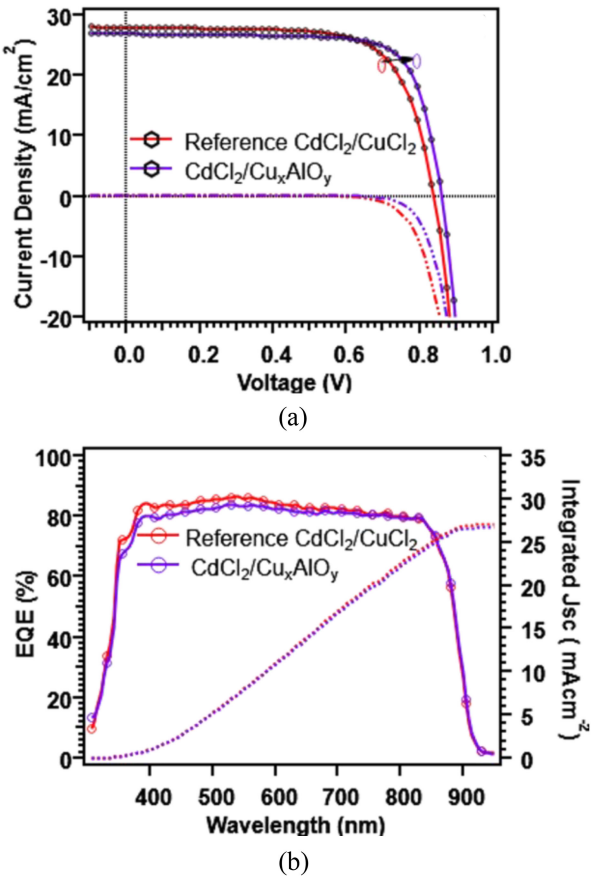

Fig. 4. (a) *J–V* characteristics of champion cells. (b) EQE plots and integrated current density curves.

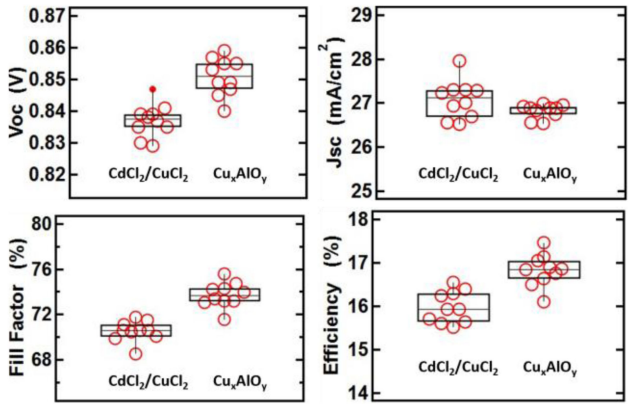

Fig. 5. Box plots of *J–V* parameters averaged for ten best cells.

with Cu_xAlO_y is slightly lower than the reference device. This suggests either that the doping near the front of the device may be slightly different, or that the addition of the buffer layer alters the optical properties of the entire stack resulting in slight increase in the reflection at the shorter wavelengths. Surprisingly, the long wavelength response is not enhanced, as expected for better collection of carriers generated more deep in the device. These issues and other aspects of the device performance with the Cu_xAlO_y passivation layer will be the subject of future studies.

IV. Conclusion

In this article, we studied that back-surface passivation with a solution processed back buffer Cu_xAlO_y on CdSe/CdTe devices. Noticeably increased PL intensity, carrier lifetime >650 ns, and increased V_{oc} indicate that the Cu_xAlO_y buffer reduces recombination at the back interface. Further, the role of Cu diffusion is distinct from that of the devices where Cu is intentionally applied at the back. Further characterization of the device stacks with back-buffer layer are needed to determine the critical Cu diffusion, electronic process at the interface and bulk, and to better understand the passivation mechanisms.

Acknowledgment

The U.S. Government is authorized to reproduce and distribute reprints for Governmental purposes not withstanding any copyright notation thereon. The authors thank Derk Rading of INTOF GmbH for TOF SIMS data.

References

[1] N. R. Paudel and Y. Yan, "Enhancing the photo-currents of cdte thin-film solar cells in both short and long wavelength regions," *Appl. Phys. Lett.*, vol. 105, no. 18, 2014, Art. no. 183510.
[2] D. Kuciauskas *et al.*, "Microsecond carrier lifetimes in polycrystalline CdSeTe heterostructures and in CdSeTe thin film solar cells," in *Proc. 47th IEEE Photovolt. Specialists Conf.*, Jun.–Aug. 2020, pp. 82–84.
[3] A. H. Munshi *et al.*, "Polycrystalline CdSeTe/CdTe absorber cells with 28 mA/cm^2 short-circuit current," *IEEE J. Photovolt.*, vol. 8, no. 1, pp. 310–314, Jan. 2018.
[4] R. M. Geisthardt, M. Topic, and J. R. Sites, "Status and potential of CdTe solar-cell efficiency," *IEEE J. Photovolt.*, vol. 5, no. 4, pp. 1217–1221, Apr. 2015.
[5] M. Green *et al.*, "Solar cell efficiency tables (version 57)," *Prog. Photovolt., Res. Appl.*, vol. 29, no. 1, pp. 3–15, 2020.
[6] A. Kanevce, M. O. Reese, T. M. Barnes, S. A. Jensen, and W. K. Metzger, "The roles of carrier concentration and interface, bulk, and grain-boundary recombination for 25% efficient CdTe solar cells," *J. Appl. Phys.*, vol. 121, no. 21, 2017, Art. no. 214506.
[7] D. Kuciauskas, J. Moseley, and C. Lee, "Identification of recombination losses in CdSe/ CdTe solar cells from spectroscopic and microscopic time-resolved photoluminescence," *Sol. RRL*, vol. 5, no. 4, 2021, Art. no. 2000775.
[8] G. K. Liyanage, A. B. Phillips, F. K. Alfadhili, R. J. Ellingson, and M. J. Heben, "The role of back buffer layers and absorber properties for >25% efficient CdTe solar cells," *ACS Appl. Energy Mater.*, vol. 2, no. 8, pp. 5419–5426, 2019.
[9] T. Ablekim *et al.*, "Exceeding 200-ns lifetimes in polycrystalline CdTe solar cells," *Sol. RRL*, vol. 5, 2021, Art. no. 2100173.
[10] F. K. Alfadhili *et al.*, "Controlling band alignment at the back interface of cadmium telluride solar cells using ZnTe and Te buffer layers," *MRS Adv.*, vol. 4, no. 16, pp. 913–919, 2019.
[11] F. K. Alfadhili *et al.*, "Potential of CdZnTe thin film back buffer layer for CdTe solar cells," in *Proc. IEEE 46th Photovolt. Specialists Conf.*, Jun. 2019, pp. 140–143.
[12] D. Pokhrel, E. Bastola, A. B. Phillips, M. J. Heben, and R. J. Ellingson, "Aspect ratio controlled synthesis of tellurium nanowires for photovoltaic applications," *Mater. Adv.*, vol. 1, no. 8, pp. 2721–2728, 2020.
[13] S. S. Bista *et al.*, "ZnTe back buffer layer to enhance the efficiency of CdS/ CdTe solar cells," in *Proc. IEEE 46th Photovolt. Specialists Conf.*, Jun. 2019, pp. 0499–0502.
[14] J. M. Kephart *et al.*, "Sputter-deposited oxides for interface passivation of CdTe photovoltaics," *IEEE J. Photovolt.*, vol. 8, no. 2, pp. 587–593, Feb. 2018.
[15] F. Werner *et al.*, "Oxidation as key mechanism for efficient interface passivation in Cu(In,Ga)Se_2 thin-film solar cells," *Phys. Rev. Appl.*, vol. 13, no. 5, 2020, Art. no. 054004.
[16] C. L. Perkins *et al.*, "Interfaces between CdTe and ALD Al_2O_3," *IEEE J. Photovolt.*, vol. 8, no. 6, pp. 1858–1861, Jun. 2018.

[17] B. Hoex, S. B. S. Heil, E. Langereis, M. C. M. van de Sanden, and W. M. M. Kessels, "Ultralow surface recombination of c-Si substrates passivated by plasma-assisted atomic layer deposited Al_2O_3," *Appl. Phys. Lett.*, vol. 89, no. 4, 2006, Art. no. 042112.

[18] A. H. Munshi, A. H. Danielson, A. Kindvall, K. Barth, and W. Sampath, "Investigation of sputtered oxides and p+ Back-contact for polycrystalline CdTe and CdSeTe photovoltaics," in *Proc. IEEE 7th World Conf. Photovolt. Energy Convers., 45th IEEE Photovolt. Specialists Conf., 28th Proc. Eur. Photovolt. Solar Energy Conf. Exhib., 34th Proc. Eur. Photovolt. Solar Energy Conf. Exhib.*, Jun. 2018, pp. 3009–3012.

[19] F. K. Alfadhili *et al.*, "Back-Surface passivation of CdTe solar cells using solution-processed oxidized aluminum," *ACS Appl. Mater. Interfaces*, vol. 12, no. 46, pp. 51337–51343, 2020.

[20] D. Kuciauskas, J. Moseley, P. Ščajev, and D. Albin, "Radiative efficiency and charge-carrier lifetimes and diffusion length in polycrystalline CdSeTe heterostructures," *Physica Status Solidi Rapid Res. Lett.*, vol. 14, no. 3, 2019, Art. no. 1900606.

[21] K. K. Subedi *et al.*, "Enabling bifacial thin film devices by developing a back surface field using Cu_xAlO_y," *Nano Energy*, vol. 83, 2021, Art. no. 105827.

[22] T. Song, A. Kanevce, and J. R. Sites, "Emitter/absorber interface of CdTe solar cells," *J. Appl. Phys.*, vol. 119, no. 23, 2016, Art. no. 233104.

[23] T. A. M. Fiducia *et al.*, "Understanding the role of selenium in defect passivation for highly efficient selenium-alloyed cadmium telluride solar cells," *Nat. Energy*, vol. 4, no. 6, pp. 504–511, 2019.

[24] E. Bastola *et al.*, "Open-circuit voltage exceeding 840 mV for all-sputtered CdS/ CdTe devices," in *Proc. 47th IEEE Photovolt. Specialists Conf.*, Jun.–Aug. 2020, pp. 2513–2518.

[25] D. Kuciauskas, J. Moseley, P. Ščajev, and D. Albin, "Radiative efficiency and charge-carrier lifetimes and diffusion length in polycrystalline CdSeTe heterostructures," *Physica Status Solidi Rapid Res. Lett.*, vol. 14, no. 3, 2020, Art. no. 1900606.

[26] U. Rau, B. Blank, T. C. M. Müller, and T. Kirchartz, "Efficiency potential of photovoltaic materials and devices unveiled by detailed-balance analysis," *Phys. Rev. Appl.*, vol. 7, no. 4, 2017, Art. no. 044016.

[27] A. B. Phillips *et al.*, "Understanding and advancing bifacial thin film solar cells," *ACS Appl. Energy Mater.*, vol. 3, no. 7, pp. 6072–6078, 2020.

[28] X. Zheng *et al.*, "Recombination and bandgap engineering in CdSeTe/ CdTe solar cells," *APL Mater.*, vol. 7, no. 7, 2019, Art. no. 071112.